DEVELOPMENT AND VALIDATION OF NOZZLE EROSION MODELS FOR SOLID AND HYBRID ROCKETS IN THE ESPSS LIBRARIES

Marco Rotondi [(1)(*)], Pierluigi Concio [(1)(#)], Simone D'Alessandro [(1)(§)], Fernando R. Lucas [(2)], Daniele Bianchi [(1)($)], Francesco Nasuti [(1)(&)], and Johan Steelant [(3)]

[(1)] Department of Mechanical and Aerospace Engineering, Sapienza University of Rome, Rome, Italy, Email: [(*)] marco.rotondi@uniroma1.it, [(#)] pierluigi.concio@uniroma1.it, [(§)] simone.dalessandro@uniroma1.it, [($)] daniele.bianchi@uniroma1.it, [(&)] francesco.nasuti@uniroma1.it
[(2)] Empresarios Agrupados Internacional, Madrid, Spain, Email: frlucas@empre.es
[(3)] Flight Vehicles and Aerothermodynamics Engineering, ESTEC-ESA, Noordwijk, Netherlands, Email: Johan.Steelant@esa.int

KEYWORDS: nozzle erosion, solid rocket motors, hybrid rocket engines, ablative materials

ABSTRACT:

Rocket nozzle throats are subjected to a harsh thermal and chemical environment, hence a proper thermal protection system (TPS) is usually employed to protect the underlying structure from the high heat flux incoming. Concerning solid and hybrid rocket applications, a wide-spread solution is to use ablative TPS. However, ablative materials are normally subjected to a thermochemical erosion process, leading to the nozzle throat enlargement and thus to a specific impulse loss and to a modified thrust curve. For this reason, reliable numerical models are required to accurately predict nozzle erosion and the associated engine performance losses. A low order representation of such complex phenomenology might represents a useful tool during the engine design phase. In this context, the present work aims to improve the solid/hybrid thrust chamber components already available in the European Space Propulsion System Simulation (ESPSS) framework by including nozzle erosion prediction capabilities. Three different reduced ablation models have been identified, implemented, and validated by means of CFD simulations and experimental data available in the literature, highlighting the improved performance prediction capabilities of the ESPSS libraries.

1. INTRODUCTION

Carbon-based ablative materials are commonly used in propulsive nozzles of solid rocket motors (SRM) and hybrid rocket engines (HRE) as thermal protection systems (TPS) because of their excellent thermal and physical properties. The carbon-based nozzle surface recedes because of the chemical and mechanical interaction with the hot exhaust gases, increasing the nozzle throat area and resulting in a performance loss. The description and modeling of the major physical mechanisms governing the erosion and the thermophysical behavior of the TPS are therefore of fundamental importance.

In the open literature, different high-fidelity numerical approaches to the nozzle ablation problem can be retrieved, ranging from ablative one-dimensional and multi-dimensional material response codes [1-3] to finite-rate ablative boundary conditions and gas-surface interaction (GSI) models integrated in Computational Fluid Dynamics (CFD) solvers [4-16]. However, few low order representation of the nozzle erosion phenomenon, such as analytical or semi-empirical models, are currently available. A low order representation of a complex phenomenology such as the nozzle ablation problem might represents a useful tool during the engine design phase, in order to have a quick (even if approximated) evaluation of this sophisticated phenomenon.

The simplest approaches to the nozzle erosion problem are represented by analytical and semi-empirical models. The literature contains relatively few exact analytical solutions of the heat conduction equation in which phase changes and the associated latent heat are considered, such as in the case of an ablative TPS. In the 60's, Baer and Ambrosio [17] dealt with the problem of heat conduction with sublimation/phase change at the surface (i.e., surface recession). However, the analytical solutions proposed in [17] have an important limitation in the possibility to handle only constant recession rates and/or constant incoming heat fluxes. Semi-empirical correlations for SRM [18,19] and HRE [20,21] nozzle throat erosion are instead able to take into account the main functional dependencies of the ablation phenomenon, such as propellant composition and chamber pressure. However, they are limited to few specific applications in terms of propellant combinations, and cannot be employed in a more general case.

In the mid to late 60's, the CMA (Charring Material Ablation) material response code [1] has been developed. CMA is a thermochemical ablative material response code based on the so called

equilibrium B' tables model which has been the reference NASA ablative code until the late 90's. The B' tables employed in the CMA numerically represent a general ablation function for a specific TPS material and a specific boundary-layer edge gas, and may be potentially used as a reduced nozzle erosion model in propulsive system analysis tools. The CMA model relies on a heat and mass transfer coefficient formulation [22,23], hence simplifying assumptions are necessarily needed, including semi-empirical correlations in order to take into account geometrical and/or chemical side effects (e.g., nozzle throat radius and blowing). Moreover, the B' tables are usually computed assuming chemical equilibrium between the solid material surface and the external boundary-layer edge gas, which is a reasonable assumption only under the diffusion-limited ablation regime (i.e., extremely fast surface reactions) [7]. Hence, the equilibrium B' tables model cannot be employed in case of kinetic-limited ablation regimes, such as for most HRE [11].

Recently, an interesting simplified ablation model, able to take into account surface chemistry phenomena including finite-rate effects, has been proposed in [24]. The method has been developed for a propulsive system analysis code used for SRM preliminary design, hence fully based on reduced models. However, the main limitation of the proposed methodology is the lack in prediction of the boundary layer effects on chemistry, leading to possible reliable results only in case of strongly kinetic-limited ablation regimes.

In this context, the present work aims to improve the solid/hybrid thrust chamber components already available in the European Space Propulsion System Simulation (ESPSS) framework [25,26] by including nozzle erosion prediction capabilities. Three nozzle erosion models have been selected and implemented in the ESPSS framework, and they have been validated by means of CFD simulations and experimental data available in the literature, highlighting the improved performance prediction capabilities available in the ESPSS libraries concerning solid and hybrid rocket engine simulation.

2. NUMERICAL MODELS

Three nozzle erosion models have been selected and implemented in the ESPSS framework. Models selection has been carried out considering different aspects, such as the models suitability with the ESPSS architecture, their range of applicability, and their reliability. The implementation has been carried out within the original solid/hybrid thrust chamber super-components [25], without altering in any significant way their original architecture. Hence, all the original flow models have been retained, and the ablative subroutines can be simply activated or de-activated. Throat/nozzle erosion and shape change are accounted by updating the combustor geometry in time using specific meshing and interpolation procedures needed in order to correctly handle the time-marching nozzle geometry. Not all the models can be freely used: in fact, some models can be used only for SRM applications, while others only for HRE ones. In the following, the different models implemented are described in details.

2.1. Semi-empirical correlations

Semi-empirical correlations are a zero-dimensional model for nozzle throat erosion rate calculation. Two different semi-empirical correlations have been identified in the literature and implemented in the ESPSS framework, with specific applications to SRM [18,19] and HRE [20].

Concerning SRM, the selected semi-empirical correlation calculates nozzle throat erosion rate $\dot{r}_{th}$ as a function of chamber pressure p_c, nozzle geometrical characteristics, and concentration of water vapor in the free-stream [18,19]:

$$\dot{r}_{th} = 1.4732 \cdot 10^{-5} M_{H_2O} \left(\frac{p_c}{p_{c,ref}}\right)^{0.8} \left(\frac{D_{th_{ref}}}{D_{th}}\right)^{0.2} \left(\frac{D_{th_{ref}}}{D_{th}} \frac{R_c}{R_{c,ref}}\right)^{0.1} \left(\frac{\rho_{c,ref}}{\rho_c}\right) (1+\varphi)^{-1} \quad \text{Eq.1}$$

where M_{H_2O} is the mole percentage of water vapor in the gaseous mixture at throat, D_{th} is the nozzle throat diameter, R_c is the nozzle curvature radius, ρ_c is the ablative material char density, and φ is the pyrolysis to char mass flow rate ratio [12]. The subscript ref indicates reference quantities.

On the other hand, concerning HRE applications, the selected semi-empirical correlation calculates nozzle throat erosion rate as a function of chamber pressure, nozzle geometrical characteristics, and oxidizer-to-fuel mixture ratio (i.e., equivalence ratio) [20]:

$$\dot{r}_{th} = \frac{K_1}{\rho_c(1+\varphi)} \left[\left(\frac{3.42}{\phi}\right)^{-1.125} 10^{\left(\frac{-3.157 \cdot \phi}{3.42} - 0.1557\right)} p_c^{K_2 \left(0.00174 \left(\frac{3.42}{\phi}\right)^2 - 0.05301 \left(\frac{3.42}{\phi}\right) + 1.119\right)} \right] \quad \text{Eq.2}$$

where K_i are user-defined semi-empirical coefficients (used in order to take into account nozzle geometrical effects) and ϕ is the equivalence ratio. The inclusion of the equivalence ratio dependence is of fundamental importance as throttling and mixture ratio shift are intrinsic characteristics of HRE [11].

It is worth noting how the semi-empirical correlations just described cannot be freely used and are subjected to some constrains. In particular, Eq. 1 can be used only in case of solid grains employing metal powders (i.e., aluminum) and ammonium perchlorate as the oxidizer [18]. On the other hand, Eq. 2 is valid only for HRE in which oxygen is employed as the oxidizer [20].

The semi-empirical correlations provide only the erosion rate at nozzle throat. However, if nozzle convergent/divergent erosion is desired as well, a simple correction of the throat erosion rate in terms of the Bartz correlation [27] is performed. In particular, the throat erosion rate calculated by the semi-empirical correlations is scaled by means of the area ratio:

$$\dot{r}_i = \dot{r}_{th}(A_i/A_{th})^{-0.9} \qquad \text{Eq.3}$$

2.2. B' tables model

The B' tables model [1] relies on the coupled solution of the Surface Mass Balance (SMB) and Surface Energy Balance (SEB). Surface balances are written by employing transfer coefficients in order to capture the effects of species diffusion through the chemical boundary layer and heat transfer through the temperature boundary layer.
In the B' model, the solution of the SMB is tabulated in the so called B' thermochemical equilibrium tables. The B' parameter (or dimensionless ablation mass flux B') listed in the aforementioned tables is calculated (for a non-pyrolyzing carbon-based material) as:

$$B' = \frac{\dot{m}_w}{\rho_e u_e C_m} = \frac{Y_{kw}-Y_{ke}}{Y_{kc}-Y_{kw}} = \frac{Y_{kw}-Y_{ke}}{1-Y_{kw}} \qquad \text{Eq. 4}$$

where $\dot{m}_w$ is the overall ablation mass flux, C_m is the dimensionless mass transfer coefficient, and Y_k is the elemental mass fraction of the k-th chemical element. The subscripts w, e, and c indicate gas conditions at wall, gas conditions at the boundary-layer edge, and solid material conditions at surface, respectively. Hence, the mass fractions of the k chemical elements considered in the problem are needed in order to compute the B' tables. The computation of these mass fractions at varying wall pressures and temperatures can be carried out through a chemical equilibrium software [28]. It is worth noting how a different B' table must be generated when the environmental gas (i.e., Y_{ke}) is changed. Hence, different tables are needed for different propellant formulations. For this reason, only a limited number of tables have been included within the ESPSS libraries, covering the most diffused SRM propellant formulations.
The SEB, solved accordingly to the tabulated SMB solutions listed in the B' tables, writes as:

$$\rho_e u_e C_h(h_r - h_{ew}) + \rho_e u_e C_m(h_{ew} - h_w + B' h_{sw} - B' h_w) = \sigma \varepsilon T_w^4 + q_{cond,w} \qquad \text{Eq. 5}$$

where C_h is the dimensionless heat transfer coefficient, h_r is the recovery enthalpy, and $q_{cond,w}$ is the heat conduction term.
The dimensionless heat transfer coefficient C_h is obtained by means of the Bartz correlation. In order to take into account boundary-layer development effects in the Bartz correlation, which are of fundamental importance in ablative calculations, two correction factors have been included, taking into account wall entrance length and contraction ratio effects [29]:

$$K_a = \left(\frac{R_{in}}{L_{en}}\right)^{0.2}; \quad K_b = \left(\frac{R_{th}}{R_{in}}\right)^{0.05} \qquad \text{Eq. 6}$$

$$\rho_e u_e C_{h0} = \frac{h_{c,m}}{C_p} = \frac{h_c K_a K_b}{C_p} \qquad \text{Eq.7}$$

In Eqs. 6 and 7, h_c is the classical Bartz coefficient [27], R_{in} is the nozzle radius at nozzle inlet, and L_{en} is the wall entrance length from nozzle inlet up to throat.
As the Bartz correlation is not able to take into account the blockage effect due to the surface ablation, a blowing correction is used [1]:

$$\frac{C_h}{C_{h0}} = \frac{\zeta}{e^{\zeta}-1}; \qquad \zeta = \frac{2\,\lambda\,\dot{m}_w}{\rho_e u_e C_{h0}} \qquad \text{Eq. 8}$$

where λ is a semi-empirical parameter, typically assumed equal to 0.4 in case of turbulent flow [1].
The dimensionless mass transfer coefficient C_m is then evaluated from the knowledge of C_h by means of the Chilton-Colburn relation [1] assuming a constant Schmidt number of 0.7.
The wall temperature T_w represents the unknown of the problem, and must be numerically iterated in order to satisfy the SEB. The B' parameter is obtained by a proper interpolation inside the B' tables, using the local pressure (in a generic section of the nozzle convergent/divergent) and/or the throat pressure and the wall temperature at the current iteration. When the correct wall temperature value is obtained, the recession rate can be evaluated from the correspondent B' parameter:

$$\dot{r} = \frac{B' \rho_e u_e C_m}{\rho_c\,(1+\varphi)} \qquad \text{Eq. 9}$$

2.3. Simplified kinetic chemistry model

The simplified kinetic chemistry model (FRchem) originally proposed in [24] has been largely enriched in order to improve its applicability range as well as its overall predictive capability. In fact, the original model [24] lacks in terms of chemical boundary layer modelling, as the partial pressures of the oxidizing species at wall are assumed to be coincident to the free-stream ones. This is a good assumption only when ablation is strongly kinetic-limited, as the chemical composition inside the boundary layer is expected to be almost coincident with the boundary-layer edge one (the species are consumed slowly by the surface reactions, while the diffusion of the consumed species towards the solid wall is much more faster, preventing the presence of high spatial concentration gradients). However, when ablation is diffusion-limited, boundary layer effects on the chemical composition becomes much more important, hence in this case the original methodology proposed in [24] is expected to overpredicts the material

ablative response. Hence, different additional features have been added to the original model in order to extend its applicability ranges. The final result is an almost fully-predictive model, quite similar to those employed in state-of-art ablative CFD codes [7,11], which relies on few semi-empirical factors modelling mass and heat transport phenomena.
In the final model, the thermochemical ablation is modelled via SMB and SEB and takes into account heterogeneous chemical reactions at the nozzle surface, and ablation species injection in the boundary layer. Surface balances are written by employing transfer coefficients (similarly to the B' tables model) to capture the effects of species diffusion through the chemical boundary layer and heat transfer through the temperature boundary layer. The surface balances write as follows:

$$\rho_e u_e C_m\,(Y_{ie} - Y_{iw}) + \dot{\omega}_i = \dot{m}_w Y_{iw} \qquad \text{Eq. 10}$$

$$\rho_e u_e C_h (h_r - h_{ew}) + \rho_e u_e C_m (h_{ew} - h_w) + \dot{m}_w h_{sw} = \dot{m}_w (h_{sw} - h_{s0}) + \dot{m}_w h_w + \sigma \varepsilon T_w^4 \qquad \text{Eq. 11}$$

where Y_i is the mass fraction of the i-th species.
The dimensionless parameters C_h and C_m are carried out similarly to the approach used in the B' tables model (see Eqs. 6, 7 and 8). Differently from the B' tables approach, surface conditions, including the surface heat fluxes and ablation rate, are determined based on a finite-rate surface reaction mechanism. In particular, the heterogeneous chemical reactions taking place at the nozzle surface are modelled by a semi-global graphite oxidation kinetics for non-porous graphite [30] (see Tab. 1). With this mechanism, the contribution to carbon erosion due to the i-th species can be expressed in kg/(s m^2) as [11]:

$$\dot{m}_{i,w} = k_j\, p_i^{\,n_j} \qquad (\text{for } i = \mathrm{H_2O}, \mathrm{CO_2}, \mathrm{OH}, \mathrm{O}) \qquad \text{Eq. 12}$$

$$\dot{m}_{i,w} = \frac{k_5\, p_i\, Z}{1 + k_6 p_i} + k_7 p_i (1 - Z); \quad Z = \left(1 + \frac{k_8}{k_7 p_i}\right)^{-1} \quad (\text{for } i = \mathrm{O_2}) \qquad \text{Eq. 13}$$

where p_i is the partial pressure (in atm) of the oxidizing species i, and k_j is the rate constant of the j-th reaction, which can be expressed by an Arrhenius type expression of the form:

$$k_j = A_j\, T_w^{\,b_j} \exp\left(-\frac{E_j}{R T_w}\right) \qquad \text{Eq. 14}$$

The overall ablation mass flux of carbon due to the surface heterogeneous reactions is finally expressed as:

$$\dot{m}_w = \dot{m}_{H2O,w} + \dot{m}_{CO2,w} + \dot{m}_{OH,w} + \dot{m}_{O,w} + \dot{m}_{O2,w} \qquad \text{Eq. 15}$$

The rate of production/consumption of the generic gas-phase species i at the nozzle surface $\dot{\omega}_i$ in Eq. 10 can be easily derived from the rate of ablation of carbon by the generic oxidizing species, Eqs. 12 and 13, and the mass balance available once the species molecular weights and the stoichiometry of the surface reactions (see Table 1) are known.
The final result from the coupling between the SMB and the finite-rate chemistry model is something similar to the B' thermochemical tables, which can be generated "on-the-fly" at each time-step without the assumption of chemical equilibrium, and for any propellant combination without limitations.
The SMB, the SEB and the finite-rate chemistry model are coupled in a non-linear fashion, hence they must be solved jointly in an iterative way. The bisection method is used. The unknows of the problem are the chemical compositions of the gaseous species at wall (Y_{iw}), the overall ablation mass flux ($\dot{m}_w$) and the wall temperature (T_w). The solution is obtained by using the local combustor pressure (in a generic section of the nozzle convergent/divergent) and/or the throat pressure, the chemical composition of the free-stream as the first-guess wall chemical composition, and a first-guess wall temperature.
Once the overall ablation mass flux $\dot{m}_w$ is obtained, the erosion rate is calculated:

$$\dot{r} = \frac{\dot{m}_w}{\rho_c\,(1+\varphi)} \qquad \text{Eq. 16}$$

3. TEST CASES AND NUMERICAL RESULTS

For the verification and validation of the reduced nozzle erosion models previously described and implemented in the ESPSS libraries, the following test cases have been considered concerning SRM applications:

i. ISPM motor [13,31]: a series of tests

Table 1: Heterogeneous rate constants of carbon with the main oxidizing species [30].

Surface reaction	j	A_j	E_j, kJ/mol	b_j	n_j
$\mathrm{C_s + H_2O \rightarrow CO + H_2}$	1	4.8 e5	288	0.0	0.5
$\mathrm{C_s + CO_2 \rightarrow 2CO}$	2	9.0 e3	285	0.0	0.5
$\mathrm{C_s + OH \rightarrow CO + H}$	3	3.61 e2	0.0	-0.5	1.0
$\mathrm{C_s + O \rightarrow CO}$	4	6.655 e2	0.0	-0.5	1.0
$\mathrm{C_s + 0.5\ O_2 \rightarrow CO}$	5	2.4 e3	125.6	0.0	0.5
	6	2.13 e1	-17.17	0.0	0.5
	7	5.35 e-1	63.64	0.0	0.5
	8	1.81 e7	406.1	0.0	0.5

employing a solid propellant without metal additives (13% HTPB, 87% Ammonium perchlorate (AP)), including different chamber pressure levels. A graphitic nozzle with a bulk density of 1920 kg/m^3 is used in all tests. Experimental averages of throat erosion rates are available for validation. Two test cases, characterized by substantially different conditions in terms of chamber pressure, have been considered (see Table 2).

Table 2: Available experimental and numerical data for the ISPM motor firings [13,31].

	Test. ISPM-01	Test. ISPM-07
D_{th}, cm	1.27	1.27
R_{in}, cm	1.0	1.0
L_{en}, cm	14.8	14.8
p_c, bar	64.4	162.8
$\dot{r}_{th}$, mm/s	0.162	0.261 (±22.6%)
η_{c*}, - [13]	0.937	0.940

ii. BATES motor [18,32]: a series of tests employing different solid propellant formulations including metal additives (HPTB, AP, and aluminum powder). A graphitic nozzle with a bulk density of 1830 kg/m^3 is used in all tests. Experimental averages of the throat erosion rate are available for validation. Three tests have been considered, whose main data are summarized in Table 3.

Table 3: Available experimental data for the BATES motor firings [18,32].

	HTPB 1510	HTPB 1810	HTPB 2110
D_{th}, cm	5.08	5.08	5.08
% Al	15	18	21
p_c, bar	69	69	69
$\dot{r}_{th}$, mm/s	0.35	0.28	0.20
Y_{H_2O}, -	0.145	0.105	0.07
η_{c*}, - [32]	0.98	0.95	0.94

iii. Hippo motor [33]: a firing test employing a metallized solid propellant (12% Poly-Butadiene Acrylo-Nitrile copolymer (PBAN), 2% of epoxy curing agent, 70% AP, and 16% aluminum powder). A carbon-phenolic nozzle is employed, with a virgin density of 1462 kg/m^3 and a char density of 1173 kg/m^3 (i.e., φ=0.246). The experimental chamber pressure trace is provided in [33] and the experimentally measured erosion all along the nozzle length is available for validation [33]. Hence, this test case can be used in order to assess the nozzle shape change capabilities included in the ESPSS libraries.

The schematics used in the ESPSS for the simulations of all the SRM test cases just described is reported in Fig. 1.
On the other hand, the following test campaigns, both carried out at the Hokkaido University [20,21], have been used for validation concerning HRE applications:

i. HDPE/LOX tests [20]: a series of 2kN thrust-class firing tests using different nozzle geometries and covering a wide range of average mixture ratio and chamber pressures conditions. A graphitic nozzle is used, with a bulk density of 1850 kg/m^3. Experimental averages of nozzle throat erosion rate are available for validation. In particular, three test cases, characterized by substantially different conditions in terms of oxidizer-to-fuel mixture ratio, have been considered (see Table 4).

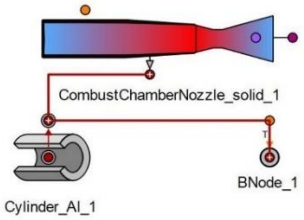

Figure 1: Schematics for SRM simulations with nozzle erosion in the EcosimPRO/ESPSS.

Table 4: Available experimental data for the HDPE/LOX tests considered [20].

	Test A-2	Test A-5	Test B-7
D_{th}, cm	2.70	2.70	1.98
R_{in}, cm	3.30	3.30	6.50
L_{en}, cm	4.01	4.01	12.03
p_c, bar	19.79	16.07	29.85
O/F, -	3.71	5.86	1.07
$\dot{r}_{th}$, mm/s	0.215 (±24.4%)	0.134 (±36.8%)	0.0 ± 0.02

ii. HDPE/N2O tests [21]: a series of 100N thrust-class firing tests covering a wide range of average mixture ratio and chamber pressures conditions. A graphitic nozzle is used, with a bulk density of 1850 kg/m^3. Experimental averages of nozzle throat erosion rate and throat wall temperature are available for validation. In particular, three test cases have been considered, briefly summarized in Table 5.

The schematics used in the ESPSS for the simulations of all the HRE test cases just described is reported in Fig. 2.
A detailed description of the main results obtained from the ESPSS libraries is reported in the following.

Table 5: Available experimental data for the HDPE/N2O tests considered [21].

	Test C-1	Test C-2	Test C-3
D_{th}, cm	0.4	0.4	0.4
R_{in}, cm	1.4	1.4	1.4
L_{en}, cm	6.4	6.4	6.4
p_c, bar	32.17	27.67	43.81
O/F, -	8.35	9.02	7.14
$\dot{r}_{th}$, mm/s	0.143 (±10.0%)	0.135 (±6.1%)	0.165 (±21.8%)

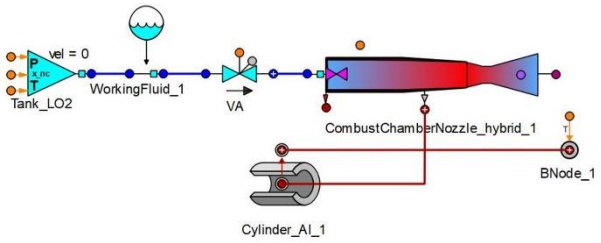

Figure 2: Schematics for HRE simulations with nozzle erosion in the EcosimPRO/ESPSS.

3.1. ISPM motor: non-metallized SRM

The first test case analyzed for the nozzle erosion models validation in SRM environment is the ISPM motor test campaign [31]. Only two nozzle erosion models have been used for the ISPM motor simulations: the B' tables model and the FRchem model. The semi-empirical correlation for SRM has not been considered as it can be used only in case of metallized solid propellants.

Table 6: Nozzle throat erosion rates obtained from the ESPSS simulations for the two ISPM motor tests considered (see Table 2) and comparison with experimental data.

$\dot{r}_{th}$, mm/s	Test ISMP-01	Test ISPM-07
exp. [30]	0.162	0.261 (±22.6%)
B' model (η_{c*}=1)	>0.64	>1.18
B' model (η_{c*}≠1)	-	-
FRchem (η_{c*}=1)	0.177 (+9.3%)	0.406 (+55.5%)
FRchem (η_{c*}≠1)	0.148 (-8.6%)	0.330 (+26.4%)

The main results obtained for the two test cases in Table 2 are summarized in Table 6.
Considering the B' tables model, extremely high throat erosion rates have been reported (even three times higher than the FRchem model ones). In fact, it is known how the equilibrium B' tables model leads to reliable results only in the diffusion-limited ablation regime, which is usually the case of SRM using metallized solid propellants [7]. Concerning the ISPM motor tests under investigation, a non-metallized solid propellant is used, and the ablation process is kinetic-limited. Hence, as expected, results obtained using the B' model are not representative of the actual physical phenomenon. This underlines how the B' model have to be used carefully.
Looking to the FRchem model results in Table 6, concerning the ISPM-01 test case, numerical and experimental data are in good agreement for both unitary and non-unitary combustion efficiencies (+9.3% and -8.6% respectively). On the other hand, concerning the ISPM-07 test case, throat erosion rate is largely overestimated when an unitary combustion efficiency is considered (+55.5%, which is outside of the ±22.6% experimental uncertainty bar). However, by including the effects of a non-unitary combustion efficiency, an acceptable agreement with the experimental data is obtained, with a +26.4% overestimation, really close to the experimental uncertainty.
In conclusion, the FRchem model can be assumed to be validated concerning SRM applications employing non-metallized solid propellants. Moreover, it has been clarified how the FRchem model is the only valuable choice for nozzle erosion simulations in case of non-metallized solid propellants.
The ISPM motor has been used in order to assess the ESPSS predictive capabilities in terms of boundary-layer development effects on the throat erosion rate. These effects are accounted thanks to the correction factors introduced in the Bartz correlation (see Eq. 6). To this purpose, ESPSS results have been compared with CFD computations available in literature [13]. In Fig. 3, wall entrance length has been made dimensionless using the actual wall entrance length L_{en} of the ISPM motor.

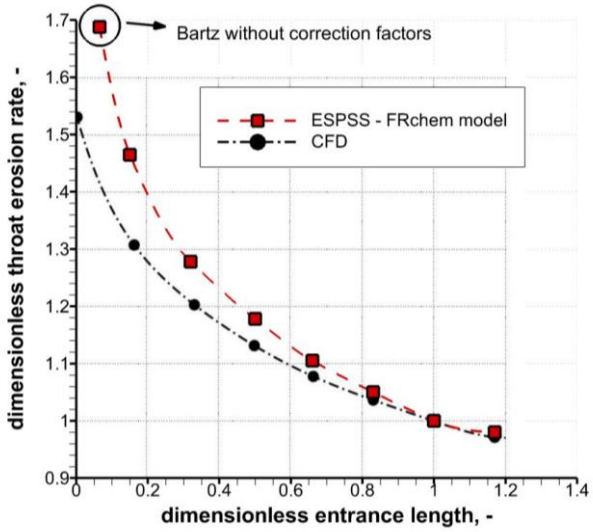

Figure 3: Wall entrance length effects on throat erosion rate according to the ESPSS and CFD simulations [13] for the ISPM motor.

The agreement between ESPSS and CFD results is really good, hence wall entrance length effects are correctly captured in EcosimPRO using the

correction factors in Eq. 6. It is worth noting how if the Bartz correlation not employing the correction factors is used, the throat erosion rate of the full wall entrance length ISPM motor is overestimated of approximately 70%. Hence, this underlines how boundary-layer development effects are of fundamental importance in ablative calculations and must be carefully taken into account.

3.2. BATES motor: metallized SRM

The second test campaign analyzed for the nozzle erosion models validation in SRM environment is the BATES motor one [18], which focuses on metallized solid propellants. Three nozzle erosion models have been used for the BATES motor simulations: the semi-empirical correlation for SRM (see Eq. 1), the B' tables model, and the (FRchem) model.

Table 7: Nozzle throat erosion rates obtained from the ESPSS simulations for the three BATES motor tests considered (see Table 3) and comparison with experimental and CFD data.

$\dot{r}_{th}$, mm/s	HTPB 1510	HTPB 1810	HTPB 2110
exp. [18]	0.35	0.28	0.20
CFD eql [8]	0.396 (+12.2%)	0.291 (+2.1%)	0.194 (-3.0%)
CFD f.r. [8]	0.349 (-1.1%)	0.274 (-3.9%)	0.193 (-3.5%)
Semi-empirical	0.373 (+5.7%)	0.295 (+3.5%)	0.210 (+5.0%)
B' model (eql.)	0.48 (+35.9%)	0.376 (+31.9%)	0.253 (+26.5%)
FRchem (f.r.)	0.33 (-6.5%)	0.301 (+5.6%)	0.261 (+30.5%)

The main results obtained for the three test cases in Table 3 are summarized in Table 7.
For all the test cases analyzed, the ESPSS model performing better with respect to the experimental data is the semi-empirical one, with a maximum discrepancy in terms of throat erosion rate of +5.7%. An interesting aspect has to be underlined by looking to the B' and FRchem model results. The erosion rates at throat computed with the chemical equilibrium approach (i.e., B' model) show a monotonically decreasing discrepancy with respect to the experimental data as the aluminum content is increased. This trend has been noticed as well in CFD computations [8]. The reason is the importance of the surface chemical kinetics in case of low aluminum contents (i.e., 15% Al, HTPB 1510), as in this case wall temperature is lower and ablation is kinetic-limited. Moving towards 18% and 21% Al, the ablation process passes gradually from being kinetic-limited to become diffusion-limited. In fact, wall temperature increases due to the higher flame temperature (ensured by the major aluminum content) and to the lower erosion rate (ensured by the lower content of oxidizing species). In case of a diffusion-limited ablation regime, results from the surface equilibrium model are expected to be more reliable. This has been observed in the CFD simulations [8] and has been confirmed as well by the ESPSS results. In fact, the erosion prediction with the finite-rate model (i.e., FRchem) is almost exactly superimposed to its surface equilibrium counterpart (i.e., B' model) in case of the higher aluminum content (i.e., 21% Al, HTPB 2110).
It is worth noting how all models are capable to correctly capture the variation of the throat erosion rate at varying solid propellant formulation. Therefore, even if slight errors in terms of throat erosion are obtained in some cases (with a maximum discrepancies of +35.9%), it can be concluded how results of the ESPSS simulations compare well with the experimental data.

3.3. Hippo motor: nozzle shape change

The last experimental test analyzed for the nozzle erosion models validation in SRM environments is the Hippo motor one [33]. This test case has been used in order to verify the reliability of the full-nozzle shape change capabilities included in the ESPSS. Two nozzle erosion models have been used for the Hippo motor simulations: the semi-empirical correlation for SRM and the FRchem model.

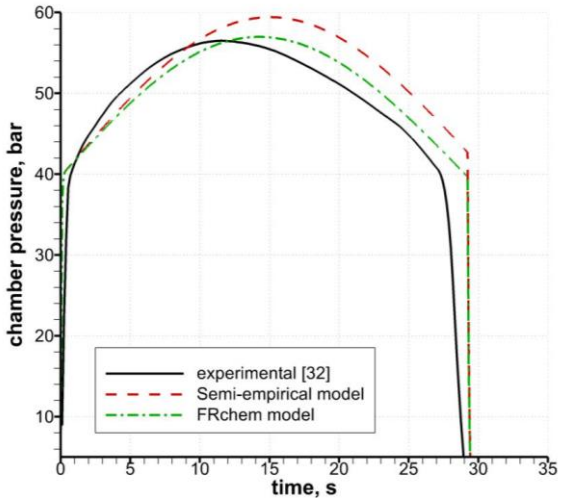

Figure 4: Comparison between the experimental chamber pressure trace and the chamber pressure time histories obtained using different ESPSS nozzle erosion models.

A first effort has been dedicated in rebuilding the experimental chamber pressure time history. In fact, as the nozzle shape change has to be predicted, a time-accurate rebuilding of the whole motor firing is required. Hence, the nozzle grain geometrical characteristics have been rebuilt in order to match as much as possible the experimental chamber pressure (including nozzle throat erosion effects). The reference ablative

model considered in the grain geometry rebuilding is the FRchem model. The chamber pressure time history obtained is reported in Fig. 4. It is worth noting how a slight chamber pressure overestimation can be observed for the semi-empirical correlation model, as in this case the calculated nozzle throat erosion is lower (see Fig. 5). Anyway, looking to the throat erosion rate time histories reported in Fig. 5, it can be appreciated how the calculations performed in the ESPSS are in good agreement with CFD simulations performed using an in-house RANS-based CFD solver.

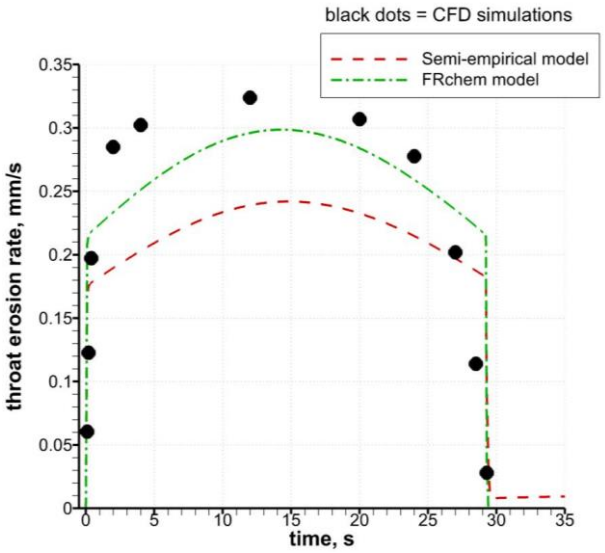

Figure 5: Comparison between nozzle throat erosion rates obtained from CFD simulations and ESPSS computations for the Hippo motor.

Figure 6 shows the erosion rate distributions along the nozzle length at different times according to CFD and ESPSS calculations. Here, it can be observed how the variations of the erosion rate distribution over time are well captured in the ESPSS, as both semi-empirical and FRchem models show an erosive behavior in time qualitatively similar to the CFD, with a maximum erosion rate at around 12 seconds.

In Fig. 7, erosion rate distributions at the initial (0.2 seconds) and final (28 seconds) times have been made dimensionless using the correspondents throat erosion rates as reference values. By doing this, the effect of the nozzle shape change on the erosion rate distribution can be more easily appreciated. All ESPSS models show a similar modification of the erosion distribution passing from the initial to the final time instant, with an increased erosion in the convergent and divergent zones relatively to the throat one. A similar behavior is obtained from ablative CFD simulations.

Results in terms of nozzle shape change according to the ESPSS libraries shows how both nozzle erosion models considered perform qualitatively well along the nozzle length with respect to

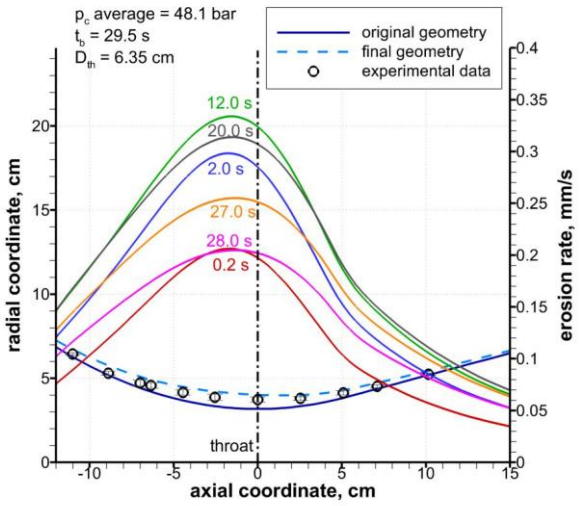

(a) CFD.

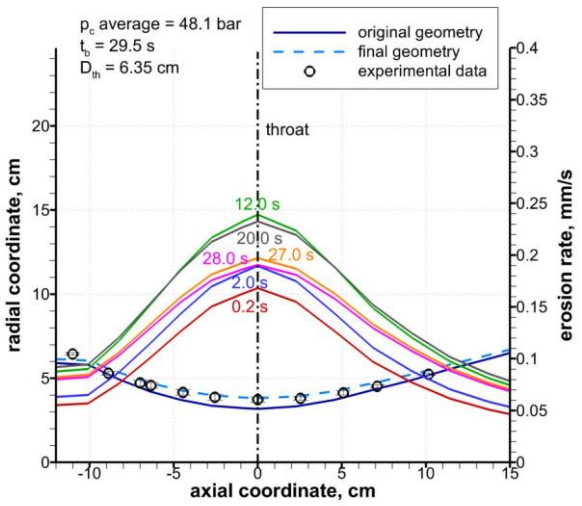

(b) ESPSS – semi-empirical.

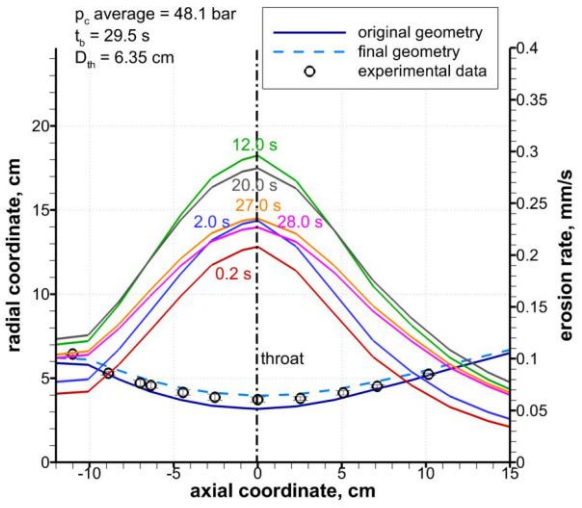

(c) ESPSS – FRchem model.

Figure 6: Erosion rate distributions along the nozzle length at different times according to CFD and ESPSS calculations and corresponding nozzle shape change.

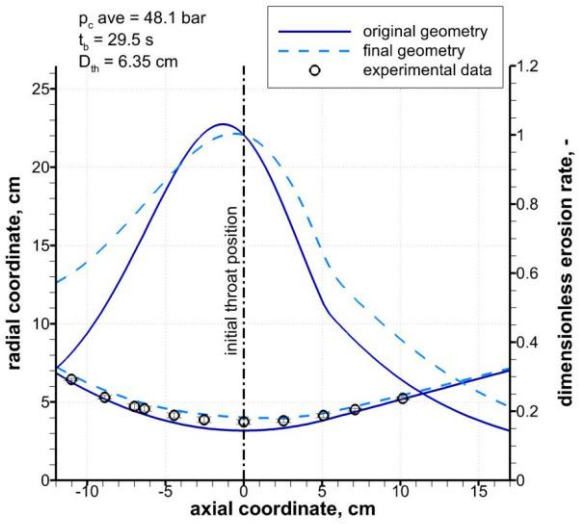

(a) CFD.

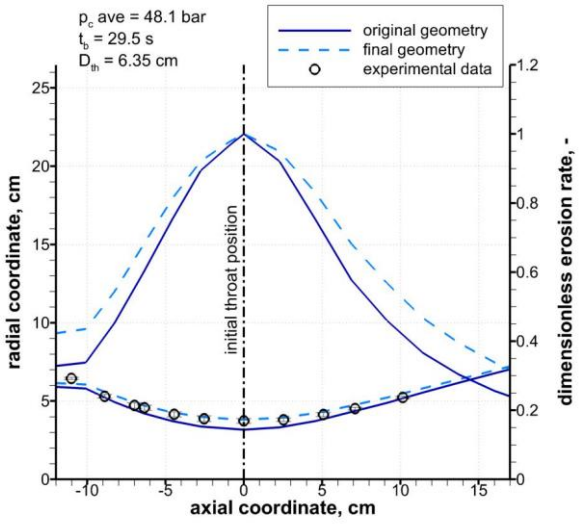

(b) ESPSS – semi-empirical.

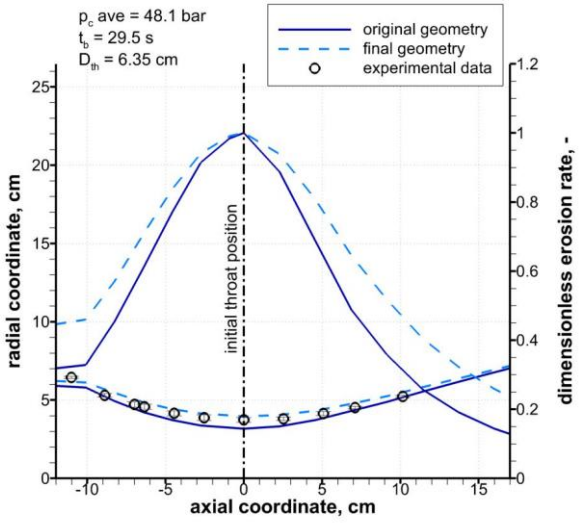

(c) ESPSS – FRchem model.

Figure 7: Dimensionless erosion rate distributions along the nozzle length at the initial (0.2 s) and final (28 s) times according to CFD and ESPSS computations.

experimental and CFD data (see Fig. 8). In particular, results obtained with the FRchem model are almost overlapped to the CFD one. On the other hand, the semi-empirical correlation model slightly underestimate the CFD results.

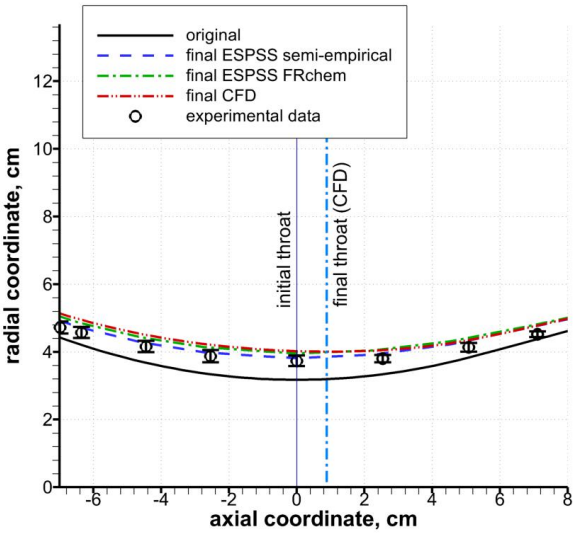

Figure 8: Hippo motor shape change according to ESPSS nozzle erosion models and CFD simulations and comparison with the experimental data.

3.4. HDPE/LOX tests

The first test campaign analyzed for the nozzle erosion models validation in HRE environment employs HDPE as the fuel and LOX (i.e., liquid oxygen) as the oxidizer [20]. A selection of three tests has been considered for the validation (see Table 4), ranging from extremely fuel-rich conditions (i.e., test B-7) to oxidizer-rich conditions (i.e., test A-5). In this way, the capability of the ESPSS ablation models in dealing with different flow conditions in terms of equivalence ratio can be assessed. Two nozzle erosion models have been used in the simulations: the semi-empirical correlation for HRE and the FRchem model.

In Fig. 9, results in terms of throat erosion rate and wall temperature are summarized for the three test conditions in Table 4. Concerning throat erosion rates (see Fig. 9(a)), ESPSS models shows a good capability of reproducing the ablative behavior at varying oxidizer-to-fuel mass ratio. In particular, for test B-7 (i.e., fuel-rich conditions), an almost null throat erosion has been computed with all the ESPSS models tested, even if chamber pressure is quite high. Experimental evidences and CFD data confirm this result. Instead, looking to near stoichiometric conditions (i.e., Test A-2), an high throat erosion rate has been obtained. The empirical correlation result is almost superimposed to the experimental and CFD data, while the FRchem model slightly overestimates them, even if remaining significantly close to the experimental uncertainty bar. The considerations made for Test

A-2 applies for Test A-5 as well (i.e., oxidizer-rich conditions). On the other side, concerning throat wall temperature (see Fig. 9(b)), ESPSS results are quite in line with CFD data, except for Test B-7, for which a +14.5% overestimation is observed.
In conclusion, qualitative variations of both throat erosion rate and wall temperature at varying oxidizer-to-fuel mass ratio and chamber pressure in HRE are successfully captured by the ESPSS erosion models employing oxygen as the oxidizer.

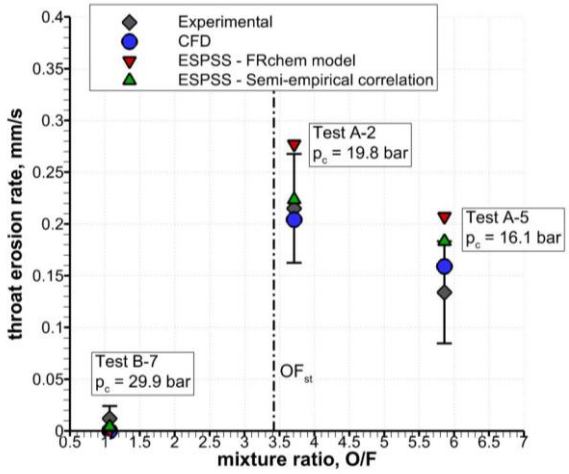

(a) Throat erosion rate.

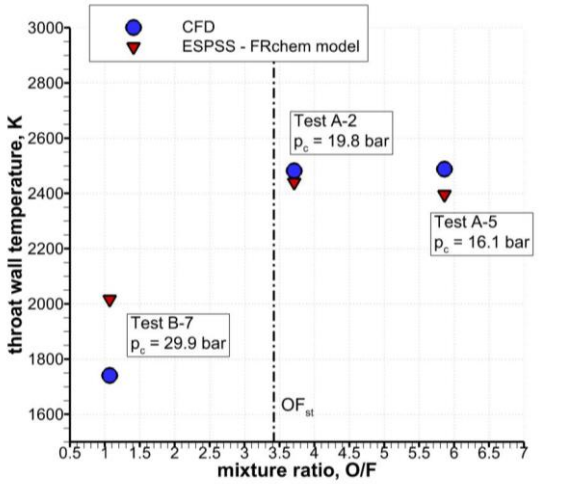

(b) Throat wall temperature.

Figure 9: Throat erosion rate and wall temperature obtained from ESPSS for the HDPE/LOX tests (see Table 4) and comparison with experimental data and CFD computations.

3.5. HDPE/N2O tests

The second test campaign analyzed for the nozzle erosion models validation in HRE environment employs HDPE as the fuel and N2O (i.e., nitrous oxide) as the oxidizer [21]. A selection of three tests has been considered for the validation (see Table 5), consisting in a fuel rich test case (Test C-3), and two near stoichiometric test cases (Test C-1 and C-2). Only the FRchem model has been used, as the semi-empirical correlation for HRE is valid only if oxygen is used as the oxidizer.
In Fig. 10, results in terms of throat erosion rate and wall temperature are summarized for all the three test conditions in Table 5. Concerning throat erosion rates (see Fig. 10(a)), the ESPSS FRchem model show to well reproducing the ablation behavior at varying oxidizer-to-fuel mass ratio. In particular, results are always inside the experimental uncertainty bar. On the other side, concerning throat wall temperature (see Fig. 10(b)), ESPSS results are quite in line with experimental and CFD data for all the test cases analyzed.

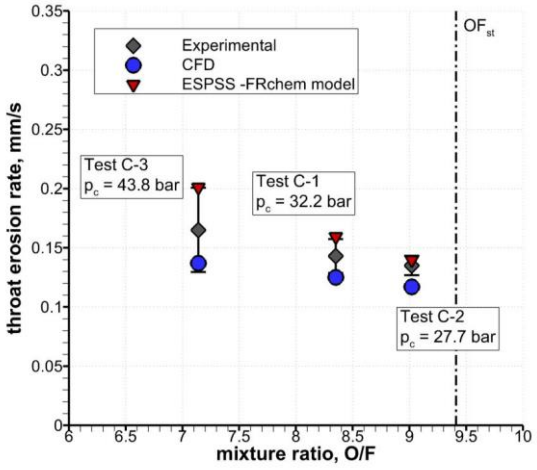

(a) Throat erosion rate.

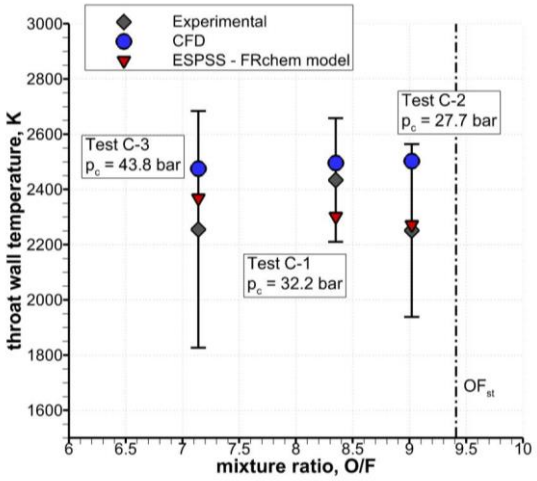

(b) Throat wall temperature.

Figure 10: Throat erosion rate and wall temperature obtained from ESPSS for the HDPE/N2O tests (see Table 5) and comparison with experimental data and CFD computations.

Therefore, it can be stated that the qualitative variations of both throat erosion rate and wall temperature at varying oxidizer-to-fuel mass ratio and chamber pressure are successfully captured. In particular, this confirms the extremely flexible applicability of the FRchem model, which is the

only nozzle erosion model included in the ESPSS libraries which can be used for both SRM and HRE applications without any limitation in terms of propellant combination and/or composition.

4. CONCLUSIONS

A detailed review on the state of the art of ablation modelling, with particular emphasis on propulsive applications, has been presented. A major effort has been dedicated to the investigation of past and present reduced methods for ablation and nozzle erosion modelling, which could be potentially used in the ESPSS framework as an ablative subroutine. Three different ablative model have been chosen for the implementation. These models are capable of providing different accuracy-to-computational time ratios, showing a complete suitability with the ESPSS architecture. Specifically, the ablative models implemented are:

i. Semi-empirical correlation for nozzle throat ablation prediction, including two different formulations for SRM and HRE respectively (zero-dimensional model, simple and fast).
ii. B' tables model, able to provide the calculation of nozzle throat ablation and heating all along the nozzle length. The surface chemical equilibrium assumption is employed (one-dimensional model, accurate in the diffusion-limited ablation regime).
iii. Simplified kinetic chemistry model, able to provide the calculation of nozzle throat ablation and heating all along the nozzle length and reliable in both diffusion and kinetic-limited ablation regimes thanks to the inclusion of heterogeneous surface finite-rate reactions (one-dimensional model).

The implementation of the nozzle erosion models has been carried out within the original ESPSS solid/hybrid thrust chamber super-components, without altering in any significant way their original architecture. New features include ablation models as well as meshing and geometrical functions needed in order to handle the time-marching nozzle geometry.

All the models have been successfully validated by comparison among ESPSS results, experimental data, and CFD computations. Moreover, the expected limits of applicability of some models have been underlined and explained during the validation procedure.

In particular, concerning SRM applications, three different test campaigns have been analyzed. In the analysis of the ISPM motor test campaign it has been underlined how the equilibrium B' tables model cannot be used in case of non-metallized solid propellants, as in this case ablation is kinetic-limited. The BATES motor test campaign allowed for the validation of all the models implemented concerning metallized solid propellants. Moreover, it has been underlined how the equilibrium B' model leads to more and more reliable results as the solid grain aluminum content is increased due to the establishment of a diffusion-limited ablation regime. The analysis of the Hippo motor allows for the validation of the full-nozzle shape change capabilities included in the nozzle erosion models implemented. Nozzle geometry in-time evolution and the associated shape change effects on the nozzle erosion rate distribution over time have been correctly predicted by ESPSS computations.

On the other side, concerning HRE applications, two different test campaigns have been analyzed (i.e., HDPE/LOX and HDPE/N2O tests). In both cases, the models employed have shown to be able to reproduce the expected ablation behavior at varying chamber pressure and, most important, at varying oxidizer-to-fuel mass ratio. In fact, throttling and mixture ratio shift are a peculiar characteristic of HRE, altering the ablation process. In particular, all the models are able to correctly predict an almost null erosion (even in case of quite high chamber pressures) when strongly fuel-rich conditions are encountered, while providing higher erosion rates at near-stoichiometric and oxidizer-rich conditions.

ACKNOWLEDGEMENTS

This research has been supported by European Space Agency (ESA), within the frame of Contract No. 4000129564/19/NL/MG.

REFERENCES

[1] R. Kendall, R. Rindal, C. Moyer and E. Bartlett, Aerotherm charring material thermal response and ablation program: Verosion 3, 1970.

[2] J. Lechaud, T. Magin, I. Cozmuta and N. Mansour, A short review of Ablative-Material Response Models and simulation Tools, *7th Aerothermodynamics Symposium*, 2011.

[3] P. G. Cross and I. D. Boyd, Two-Dimensional Modeling of Ablation and Pyrolysis with Application to Rocket Nozzles, *Journal of Spacecraft and Rockets*, vol. 54, no. 1, pp. 212-224, 2017.

[4] K. K. Kuo and S. T. Keswani, A Comprehensive Theoretical Model for Carbon-Carbon Composite Recession, *Combustion Science and Technology* , vol. 42, no. 3-4, p. 145-164, 1985.

[5] S. T. Keswani and K. K. Kuo, Validation of an Aerothermochemical Model for Graphite Nozzle Recession and Heat-Transfer Processes, *Combustion Science and Technology*, vol. 47, no. 3-4, pp. 177-192, 1986.

[6] P. Thakre and V. Yang, Chemical Erosion of Carbon-Carbon/Graphite Nozzles in Solid-Propellant Rocket Motors, *Journal of Propulsion and Power*, vol. 24, no. 4, pp. 822-833, 2008.

[7] D. Bianchi, F. Nasuti and E. Martelli, Coupled Analysis of Flow and Surface Ablation in Carbon-Carbon Rocket Nozzles, *Journal of Spacecraft and Rockets*, vol. 46, no. 3, pp. 492-500, 2009.

[8] D. Bianchi, F. Nasuti, M. Onofri and E. Martelli, Thermochemical Erosion Analysis for Graphite/Carbon-Carbon Rocket Nozzles, *Journal*

of Propulsion and Power, vol. 27, no. 1, pp. 197-205, 2011.
[9] F. Nasuti and D. Bianchi, Carbon-Carbon Nozzle Erosion and Shape-Change Effects in Full-Scale Solid-Rocket Motors, *Journal of Propulsion and Power*, vol. 28, no. 4, pp. 820-830, 2012.
[10] A. Turchi, D. Bianchi, P. Thakre, F. Nasuti and V. Yang, Radiation and Roughness Effects on Nozzle Thermochemical Erosion in Solid Rocket Motors, *Journal of Propulsion and Power*, vol. 30, no. 2, pp. 314-324, 2014.
[11] D. Bianchi and F. Nasuti, Numerical Analysis of Nozzle Material Thermochemical Erosion in Hybrid Rocket Engines, *Journal of Propulsion and Power*, 2013.
[12] D. Bianchi, A. Turchi, F. Nasuti and M. Onofri, Chemical Erosion of Carbon- Phenolic Rocket Nozzles with Finite-Rate Surface Chemistry, *Journal of Propulsion and Power*, vol. 29, no. 5, pp. 1220-1230, 2013.
[13] D. Bianchi and F. Nasuti, Navier–stokes simulation of graphite nozzle erosion at different pressure conditions, *AIAA Journal*, 2015.
[14] D. Bianchi, L. Kamps, F. Nasuti and H. Nagata, Numerical and Experimental Investigation of Nozzle Thermochemical Erosion in Hybrid Rockets, *53rd AIAA/SAE/ASEE Joint Propulsion Conference*, 2017.
[15] D. Bianchi and A. Neri, Numerical Simulation of Chemical Erosion in Vega Solid-Rocket-Motor Nozzles, *Journal of Propulsion and Power*, vol. 34, no. 2, pp. 482-498, 2018.
[16] D. Bianchi, M. T. Migliorino, F. Nasuti and M. Onofri, CFD Analysis of Paraffin- Based Hybrid Rockets with Coupled Nozzle Erosion Characterization, *AIAA Paper*, no. 2019-4263, 2019.
[17] D. Baer and A. Ambrosio, Heat Conduction in a semi-infinite slab with sublimation at the surface, *Planetary and Space Science*, vol. 4, pp. 436-446, 1961.
[18] R. Geisler and C. Beckman, The History of the Bates Motors at the Air Force Rocket Propulsion Laboratory, *34th AIAA/ASME/SAE/ASEE Joint Propulsion Conference*, 1998.
[19] E. Cavallini, D. Bianchi and B. Favini, Internal Ballistics Modeling of High Performance SRMs with Coupled Nozzle Erosion Characterization, *47th AIAA/ASME/SAE/ASEE Joint Propulsion Conference*, 2011.
[20] D. Bianchi, M.T. Migliorino, M. Rotondi, L.T. Kamps, and H. Nagata, Numerical analysis of nozzle heating and erosion in hybrid rockets and comparison with experiments, *AIAA Propulsion and Energy 2020 Forum*, 2020.
[21] M. Rotondi, M.T. Migliorino, D. Bianchi, L.T. Kamps, and H. Nagata, Numerical analysis of nozzle transient heating and erosion in hybrid rockets burning HDPE, *AIAA Propulsion and Energy 2021 Forum*, 2021.
[22] R. Kendall, R. Rindal and E. Bartlett, Thermochemical Ablation, *AIAA Thermophysics Specialist Conference*, AIAA 65-642, 1965.
[23] L. Lees, Convective Heat Transfer With Mass Addition and Chemical Reactions, *Third AGARD Colloquim on Combustion and Propulsion*, 1959.
[24] F. Untem, F. Calciolari, L. de Almeida, G. Murari and W. Silva, A Fast Method for Preliminary Evaluation of Chemical Erosion on a Composite Nozzle, *4th Brazilian Conference on Composite Materials*, 2018.
[25] J. Moral, F. Rodriguez, J. Vilà, F. Di Matteo, J. Steelant, 1-D Simulation of Solid and Hybrid Combustors with EcosimPro/ESPSS, *Space Propulsion Conference 2014*, 2014.
[26] J. Vilá, J. Moral, V. Fernández-Villacé, and J. Steelant, An Overview of the ESPSS Libraries: Latest Developments and Future**,** *Space Propulsion Conference 2018***,** 2018.
[27] D. R. Bartz, A Simple Equation for Rapid Estimation of Rocket Nozzle Convective Heat Transfer Coefficients, *Journal of Jet Propulsion*, vol. 27, no. 1, pp. 49-53, 1957.
[28] Gordon S. and McBride B.J., Computer Program for the Calculation of Complex Chemical Equilibrium Compositions with Applications, NASA Reference Pubblication, 1311, 1994.
[29] D.R. Bartz, Turbulent boundary-layer heat transfer from rapidly accelerating flow of rocket combustion gases and of heated air, *Advances in Heat Transfer*, 1965
[30] D. Bradley, G. Dixon-Lewis, S. E. Habik and E. M. Mushi, The Oxidation of Graphite Powder in Flame Reaction Zones, *Symposium (International) on Combustion*, vol. 20, no. 1, p. 931–940, 1985.
[31] B. Evans, *Nozzle Erosion Characterization and Minimization for High Pressure Rocket Motor Applications*, Ph.D. thesis, Pennsylvania State University, 2010.
[32] R. Geisler and S. A. Kinkead, The relationship between solid propellant formulation variables and motor performance, *11th AIAA/SAE Propulsion Conference*, 1975.
[33] Arnold J., Dodson J., and Laub B., *Subscale solid motor nozzle tests (phase iv), and nozzle materials screening and thermal characterization (phase v)*, Technical Report no. CR 161254, NASA, 1979